Beckers, D. ; Ellendt, Nils ; Fritsching, Udo ; Uhlenwinkel, Volker

Impact of process flow conditions on particle morphology in metal powder production via gas atomization

Journal Article	as:	peer-reviewed accepted version (Postprint)
DOI of this document*(secondary publication):		https://doi.org/10.26092/elib/3640
Publication date of this document:		07/02/2025

* for better findability or for reliable citation

Recommended Citation (primary publication/Version of Record) incl. DOI:

D. Beckers, N. Ellendt, U. Fritsching, V. Uhlenwinkel,
Impact of process flow conditions on particle morphology in metal powder production via gas atomization,
Advanced Powder Technology, Volume 31, Issue 1, 2020, Pages 300-311, ISSN 0921-8831,
https://doi.org/10.1016/j.apt.2019.10.022.

Original Research Paper

Impact of process flow conditions on particle morphology in metal powder production via gas atomization

D. Beckers [a], N. Ellendt [a,b], U. Fritsching [a,b], V. Uhlenwinkel [a,b,*]

[a] University of Bremen, Faculty of Production Engineering, Badgasteiner Straße 1, 28359 Bremen, Germany
[b] Leibniz Institute for Materials Engineering IWT, Badgasteiner Straße 3, 28359 Bremen, Germany

ARTICLE INFO

Article history:
Received 11 December 2018
Received in revised form 16 September 2019
Accepted 23 October 2019
Available online xxxx

Keywords:
Atomization
Metal powders
Particles
CFD

ABSTRACT

Additive manufacturing processes as for instance selective laser melting or electron beam melting are becoming more common and just turning into standard manufacturing processes for metal components. Nevertheless, these processes are still new compared to classic powder metallurgy manufacturing routes such as pressing and sintering. Hence not all necessary requirements for the powders in use are fully known yet. This makes an increase in control of the powder properties a crucial task to achieve. To reach this goal one must understand the different influences on the powder production process from the beginning of the whole production route. In this work, the influence of the spray chamber flow on the particle morphology is examined. The nozzle system used to produce the metal powders is a close-coupled atomization system with a convergent-divergent gas nozzle configuration. The particle morphology as well as the particle size distribution have been analyzed to examine the influence of the atomization gas flow compared to an additional use of a coaxial gas flow. To review the changes of the flow patterns, computational fluid dynamic simulations have been performed. The particle trajectories were calculated to assess the change in particle behavior as well. Atomization experiments have been conducted with an AISI 52100 (1.3505) steel in a small batch atomization plant to evaluate the influence of the change in flow on the particle size distribution and circularity. The experimental results show that a use of additional coaxial gas leads to an increase in particle circularity up to 10% for relevant particle sizes. An approach for the quantification of satellite occurrence is given by examination of the shift of the particle size distribution to smaller diameters.

1. Introduction

Modern manufacturing processes such as selective laser melting SLM or electron beam melting EBM have high demands when it comes to powder and particle properties. A good flowability of the powder is required within the process which is determined by the shape of the particles and the amount of satellite particles sticking at the surface of larger particles. Satellite particles in the sense of this work are defined as smaller particles adhering to larger primary particles. The formation of satellite particles may be due to particle collisions or other effects during the atomization process. Research on the influence of the particle shape on bulk properties is ongoing for years due to its impact in different industry areas, e.g. pharmacy, powder metallurgy, food industry, etc. In [1] Danjo et al. examine the influence of the particle shape for organic and inorganic powders on the packing density, showing an increase in density with an increase in sphericity of the particles. Additionally, the flow behavior by means of shear strength changes. The more spherical the particles are, less shear strength is shown by the powder bed. This behavior is also examined in [2] where almost perfect spherical glass beads lead to a very low shear strength compared to other powders (i.e. TiO_2, calcite, caolin, etc.). Fu et al. [3] show the influence of shape and size of particles with three different lactose powders confirming the shape influence, as well as showing that with larger particles of the same size, the shear strength also decreases. For large particles from 100 μm to 500 μm additional information can be found e.g. in [4].

When looking at additive manufacturing processes, the used powders are typically produced via gas atomization processes. Their general advantage is the inherent tendency to produce spherical powders [5]. In gas atomization, a melt exits through an orifice and is subjected to a high velocity flow field and breaks up into

* Corresponding author at: Leibniz Institute for Materials Engineering IWT, Badgasteiner Straße 3, 28359 Bremen, Germany
E-mail address: uhl@iwt.uni-bremen.de (V. Uhlenwinkel).

droplets. The transformation of a liquid into droplets has been researched for a long time. The classification of Ohnesorge shows different modes of disintegration of a fluid jet depending on the Reynolds number and hence on the interaction with the surrounding atmosphere, from simple droplet building up to the atomization of the fluid. In [6] Lubanska is investigating the droplet size for different metal melts atomized by discrete ring nozzles, leading to a correlation between the median particle size of the spray and the ratio between gas mass flow and melt mass flow. As mentioned above, the advantage in using gas atomization is the spherical particle shape and therefore the resulting bulk properties of the powder. In [7] Fritsching is investigating the impact of the flow field on the particle shape, showing that the conditions of the atomization is influencing the particles, as well as the conditions given by the atomization chamber itself. These conditions can lead to spherical powder but also can inflict different collision effects leading to deformation and satellite formation both depending on the collision rates in the spray. Singh and Dangwal [7] are discussing various process parameters and their influence on the particle shape. They are showing that although there is a tendency to spherical particles in gas atomization due to the high surface tension of metals and the comparably low viscosity at high temperatures, one must consider other parameters as well, such as superheat of the melt or e.g. the particle size itself. It can be stated that to achieve spherical particles, the spheroidization time must be less than the solidification time of the particle (see also [8;9]). Here the spheroidization time is basically the time it takes for a melt ligament after atomization to form a spherical shape due to surface tension driven forces. As mentioned before, the sticking of satellite particles to larger particles is mainly influenced by the particle collision frequency or a particle collision probability. It can be influenced by the particle concentration in a flow. This is for example shown by Achelis [10] where a decreased particle concentration in the atomization area led to more spherical powder with less satellites for tin atomized powder.

The typical shape of a gas atomization plant is a cylindrical structure of a certain height with a conical element at the bottom of the plant (see Fig. 1). This geometry leads to a specific flow structure within the spray chamber. This structure usually can be characterized by a downward facing jet in the center of the chamber that is surrounded by a larger scale toroidal recirculation zone. This general structure is influenced by the geometry of the chamber and the use of auxiliary gas inlets in addition to the main atomizer nozzle. The general flow structure in spray chambers has already been examined and published in a variety of literature. In [11] Huang et al. analyze the flow patterns by numerical modelling for different global geometry changes of the spray chambers (e.g. hourglass, barrel, etc.) and demonstrate that all flow patterns show a toroidal recirculation zone building due to the capsuled flow created by the atomization gas flow. These authors also investigated the influence of different process parameters, such as atomization gas pressure, on the forming flow field in [12]. The influence of the chamber design is further investigated by Lampa et al. [13] who also takes the particle behavior into consideration and shows cluster formation along the spray cone boundary. This clusters also leads to a mixing process transporting particles into the recirculation field. Additionally, the behavior and distribution of particles within a spray dryer is analyzed by Mezhericher et al. [14] using a hard sphere model approach, showing the influence of the flow on the particle distribution as well as the effect of particle/particle interactions.

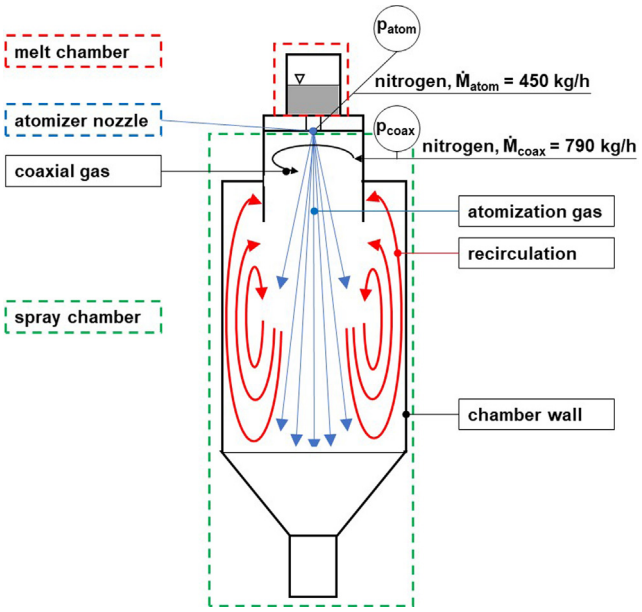

Fig. 1. Atomization plant setup with coaxial gas inlet and decreased chamber diameter near the atomization zone with $\dot{M}_{atom}$ as atomization gas mass flow and $\dot{M}_{coax}$ as coaxial gas mass flow. Resulting recirculation zone is indicated by the red arrows and the jet flow by the blue ones. (For interpretation of the references to color in this figure legend, the reader is referred to the web version of this article.)

Although a lot of research has been done in the field of spray chamber design there is a certain lack to structured approaches when it comes to the influence of the gas flow in spray chambers on the particle shape and satellites building. Also, a practical approach to quantify the change in satellites is missing so far, as well as the possibility to effectively control both effects. In this work, the influence of the spray flow structure within the spray chamber on the particle shape of metal powders is investigated by the analysis of atomization experiments with and without a coaxial gas flow. The flow pattern change itself is additionally investigated by CFD methods to get a grasp on the underlying effects influencing the particle properties. In a first step, the flow in a cylindrical chamber without coaxial gas is examined. The CFD model is validated with experimental data. Particle trajectories are calculated to show the influence of the flow on the particle behavior. The model is then extended with a coaxial gas flow used to improve the flow in the chamber resulting in changed particle properties. The coaxial flow is introduced with tangential inlets creating swirl flow conditions. An extension of the model from 2D to 3D becomes necessary due to the lack of axial symmetry. The 3D model is then used to show the influence of the swirl flow on the flow structure in the chamber. Atomization experiments with an AISI 52100 (1.3505) steel have been conducted with and without coaxial gas flow. The resulting powder properties by means of particle size and shape are compared and correlated with characteristic values from the calculated gas flow fields.

2. Experimental methods

In this work, a batch atomization plant [15] with a close-coupled nozzle system [16] has been used to analyze the gas flow patterns and velocities during melt atomization processes. For the results achieved and discussed here, the plant was further equipped with an additional coaxial gas supply system. The general configuration of the system is shown in Fig. 1.

2.1. Atomization plant

The atomization plant sketched in Fig. 1 is based on a modified pilot plant (commercial version Blue Power AU 1000) and consists of three main parts as indicated. The melt chamber is a vacuum

Table 2-1
Data of the plant geometry and the corresponding models.

		Experimental setup	2D-Model	3D-Model
Plant diameter	m	0.7	0.7	0.7
Plant height	m	4.8	4.8	4.8
Melt nozzle diameter	mm	2.5	–	–
Gas nozzle slit width	mm	0.8	–	–
Gas nozzle diameter	mm	–	4.8	4.8
Coaxial gas cross section	m^2	0.0014	–	0.0014

induction heating system. The feedstock material (here an AISI 52100 steel) is melted in an alumina crucible using a graphite susceptor for an indirect heating.

The spray chamber is mainly cylindrical except for the conical bottom part. At the bottom end a collection bin is located for the separation of coarser fractions of the powder. The top part has a smaller diameter compared to the rest of the spray chamber. This smaller area reaches into the larger diameter to create a barrier for recirculated powder to avoid back mixing of smaller particles in the atomization zone. The height of the spray chamber is 4.8 m, the height of the small diameter area is 300 mm in total (100 mm inside the large diameter area). The chamber diameter is 700 mm and the narrow part at the top is 250 mm. At the top part, 8 additional inlets for a tangential coaxial gas flow are attached to inhibit powder recirculation by influencing the gas flow within the spray chamber.

The atomization system is a close coupled gas atomizer system [16] with an annular ring slit gas nozzle with a 0.8 mm slit width at the smallest cross section for the gas flow. The system is further discussed in Section 2.3. An overview of the geometrical data is given in Table 2-1.

The exhaust outlet is located at the side of the spray chamber. A cyclone is used to separate and collect the fine powder from the exhaust gas.

The figure gives a schematic representation for the general flow pattern within the spray chamber. The blue arrows show the main spray cone and flow direction. The red arrows indicate the recirculation zone created by the entrainment of the atomization jet due to the fact of having an encased flow. The recirculation is formed in the upper part of the spray chamber (see [11,12]). At a certain point, further downstream the flow direction may change to a homogenous downstream flow across the entire chamber cross section.

2.2. Gas velocity measurements

To measure the gas velocities within the spray-chamber a pitot tube probe was used. The probe was inserted into the chamber through the cylinder wall at different nozzle distances. The depth of the measurements was varied to get velocities also at different radial positions. A schematic of the measurement area is given in Fig. 2.

The radial positions starting in the center of the chamber were varied in 50 mm steps. The outer radial position is located at 50 mm distance from the chamber wall. The top axial position for the measurements is at 100 mm from the chamber cover. The measurement time at each position was 20 s to determine an averaged velocity over time. The measurements have been done with the gas single phase without particles in the system since the results are for a validation of a single-phase model.

2.3. Nozzle system

The atomization system is a close-coupled atomizer as shown in Fig. 3. In comparison to a free-fall atomizer, the close-coupled setup can create smaller particles due to the shorter distance between the exit of the gas nozzle and the melt, but on the other hand bears the potential of melt freezing by directly cooling the melt nozzle. A more detailed and specific analysis of the nozzle system used in this work is presented in [16].

The outer coaxial gas delivery system consists of 2 × 4 cylindrical nozzles, each with a diameter of 15 mm. The nozzles are

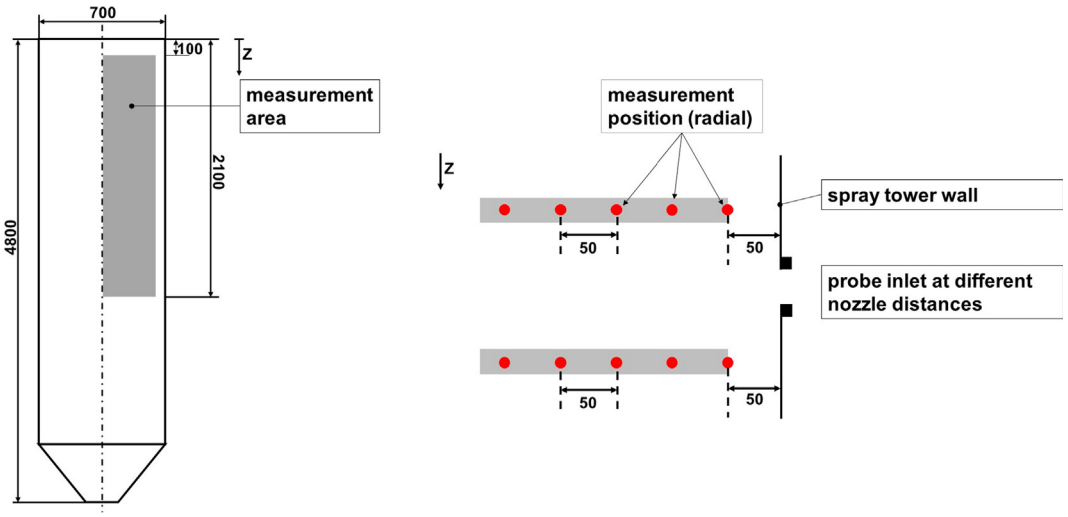

Fig. 2. Measurement area for gas velocity measurements within the atomization plant via a pitot tube anemometer. The probe position was varied in nozzle distance (left) and in radial distance from the chamber wall (right). All given measures are in mm.

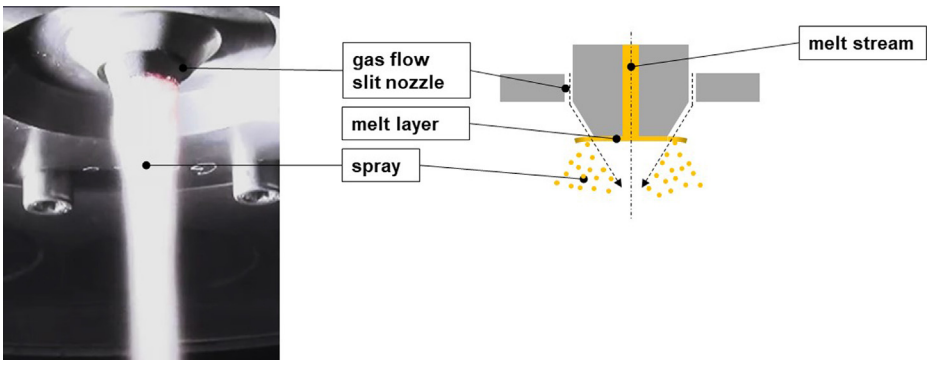

Fig. 3. Process image of a close-coupled atomizer system during the atomization of an AISI 52100 steel melt.

Table 5-1
Parameters used in the atomization experiments.

		No coaxial gas			Coaxial gas		
Feedstock	g	1624	1555	1625	1501	1561	1675
$t_{pouring}$	s	22	20	30	18	20	30
T_{atom}	–	Ambient			Ambient		
T_{coax}	–	Ambient			Ambient		
$\dot{M}_{melt}$	kg/h	266	300	195	300	281	201
GMR	–	1.69	1.5	2.31	1.5	1.6	2.24
$\dot{M}_{coax}/\dot{M}_{atom}$	–	–	–	–	1.75	1.75	1.75
$d_{50,3}$	μm	53.3	62.6	43.1	53.7	61.5	49.1
σ	–	2.6	2.71	2.26	2.71	2.77	2.47

located at the narrow section close to the atomization area and create a tangential gas flow. The resulting coaxial volume flow V_{coax} used in Table 5-1 is based on volumetric flow measurements.

2.4. Particle measurements

The measurements of the particle size and shape were done with a static particle imaging method. The measurement system was a Malvern Morphologie G3 with a 20x magnification lens. For the measurements, a sample of 2 mm^3 volume was dispersed on a glass plate resulting in a total number of about two million particles per measurement. The particles were automatically scanned, and the pictures taken during the measurement were analyzed with respect to particle shape and number size distribution. The collection of the powder is taking place directly at the bottom of the spray tower (collecting can) and in a cyclone filter in the exhaust gas system. To ensure that the sample represents the average particle composition of the powder, the preparation was done with a rotation sample divider (Retsch PT100).

For the qualitative analysis done by SEM imaging, a TESCAN VEGA3 in secondary electron scattering mode was used with 5 kV voltage.

3. Collisions

Fig. 4 illustrates the impact of the gas flow within the spray chamber on the particle morphology (shown e.g. in Section 5.2.3) in the region close to the gas nozzle and the area of particle collision due to gas recirculation.

The focus is hereby on collisions affecting the satellites on the primary particles. For the occurrence of satellites, there is usually a large particle as primary particle and smaller particles as collision

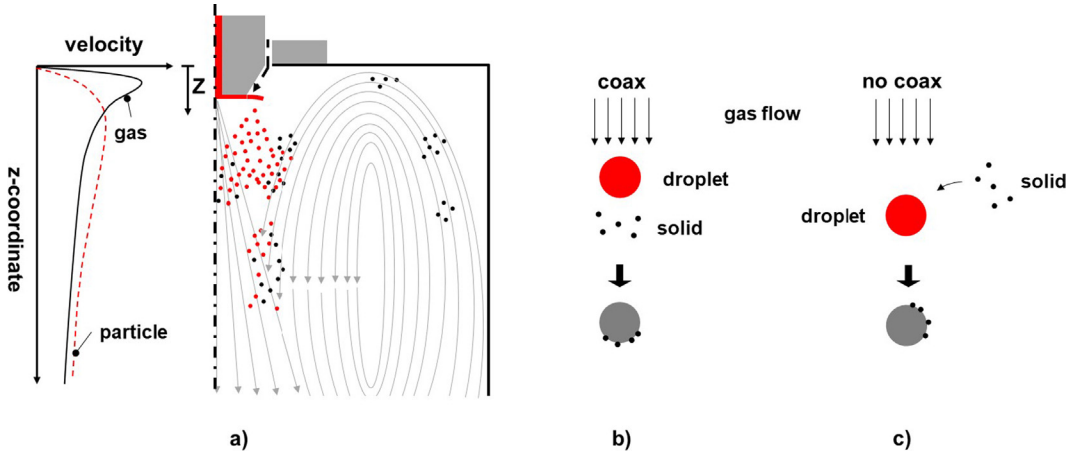

Fig. 4. Collision types within the atomization zone during the CCA due to the gas recirculation within the spray chamber.

partners. To form full aggregates after the collision, one of the colliding particles must provide the energy (here: heat) to weld or sinter the particles together. In general, two kinds of collision given by the flow pattern are given in Fig. 4. Here, the primary particle is in a semi-liquid state and therefore, smaller particles can aggregate on the surface. If the primary particle is still fully liquid, the smaller particles can fully re-melt and incorporate into the primary particle. This leads to a slight increase in particle volume but forms no satellite on the surface. If the particles have already cooled down, they would collide, and bounce off each other. For the collision (b), a newly created melt droplet is accelerated according to the graph on the left-hand side. Further downstream, the solidifying melt droplet catches smaller particles that are at a lower velocity. This can be the case due to the lower momentum of smaller particles that leads to a faster deceleration compared to large particles. Another reason is that the smaller particles are particles that are recirculated into the atomization area but not directly into the high velocity gas flow and do not undergo the same acceleration as a newly generated droplet close to the nozzle. The collision (c) is given by smaller particles recirculated into the top area of the chamber and colliding directly with a semi solid particle from the atomization zone.

Given these collision types, an alteration in the recirculation gas flow that carries the smaller particles as collision partners, can strongly influence the collision probability (e.g. due to dilution of the gas flow and influencing the particle loading) as well as the type of the collision.

4. Flow model

To evaluate the change of the flow field within the spray chamber when using the coaxial gas, a CFD model was created and the single-phase gas flow patterns have been calculated (no particle or liquid phase representing the melt stream was used here). Furthermore, the resulting flow fields were used to calculate particle trajectories to see the influence of the flow field on the particles and to gain a better understanding of the mechanisms leading to changes in the particle and powder properties. This chapter gives an overview of the model used for the calculations. The results of the calculations are shown in chapter 5.1.

4.1. Geometry and conditions

The geometry used in the model is given in Fig. 5. The inlet is located at the top of the calculation domain. The particle release zone for the particle tracking calculations is 5 mm below the melt nozzle surface and is spread across 5 mm in diameter. The outlet is given by a pressure outlet condition, located at the end of the conical chamber section at the bottom of the spray chamber. The coaxial gas inlets are modified compared to the geometry explained before. Instead of 2×4 inlets with a diameter of 15 mm each, the geometry is changed to two inlets with a coextensive cross section to keep the mass flow ratios of the gas nozzle and the coaxial gas inlets in agreement with the experiments. In general, the inlet geometries of the model are simplified compared to the physical plant. This is due to ensure stability and to decrease the calculation time. Nevertheless, the changes pose no general influence on the basic far field gas flow pattern within the spray tower.

The solver used is the CFD Solver from COMSOL Multiphysics. Here, the high Mach number flow solver for compressible flows solving the Navier-Stokes equations for mass, momentum and energy was used. The solver is a generalized minimal residual method (GMRES) which is an iterative numerical process that was developed to solve large linear equation systems and was introduced by Saad [17]. To consider turbulence, a k-epsilon turbulence model was used. This model provides good capabilities to represent the depicted process as for example shown by Rathore [18].

The initial conditions in the spray chamber were at a pressure of 0.1 MPa and a temperature of 293.15 K. The gas used is nitrogen. The inlet condition at the nozzle is based on the given total pressure derived from the experiments (see chapter 5.2), the Mach number $Ma = 1$ and the temperature at the inlet (here at 293.15 K). The outlet is pressure based and set so that there is no pressure gradient between the ambient condition of 0.1 MPa in the chamber and the outlet itself. The boundary conditions for the simulations are an over pressure of 1.25 MPa against ambient and a temperature of 293.15 K at the inlet and ambient pressure and temperature (again 293.15 K) within the spray chamber. For the particle tracking calculations, the particle density is 7.81 g/cm^3 and the particle size is varied to see the different influences

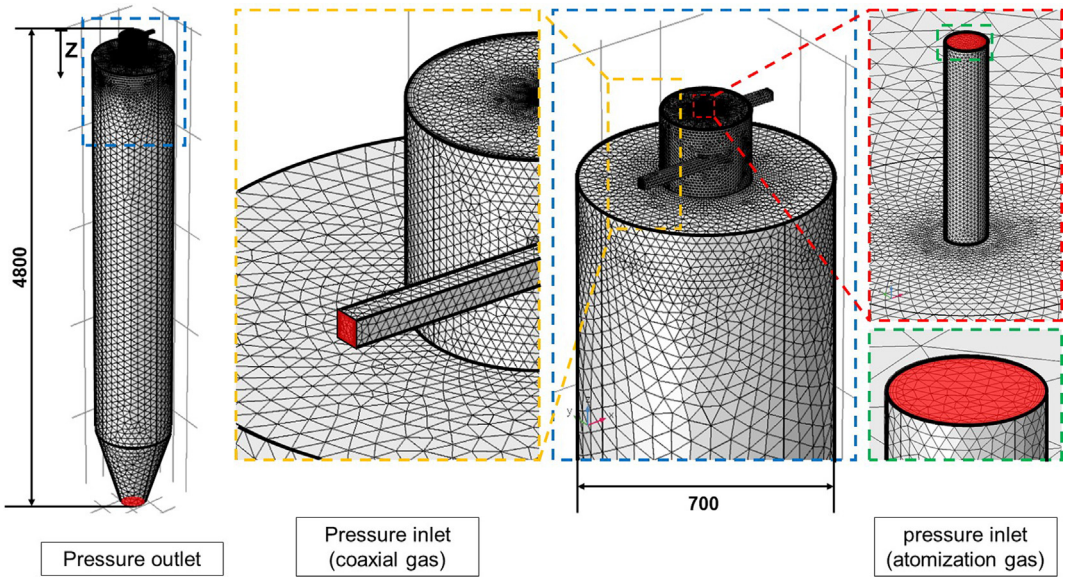

Fig. 5. Geometry and mesh of the 3D CFD model, used for the gas flow simulations with additional tangential gas inlets for a swirl flow component. The height is 4.8 m, the large diameter is 0.7 m and the small diameter is 0.25 m.

of the flow on large, medium and small (1 μm, 10 μm and 54 μm) particles. The size of the 54 μm diameter is derived from the averaged mass median diameter of the powders created in the experiments (see Table 5-1). Here, a one-way coupling approach was used. The particle drag force was calculated with the Schiller-Naumann correlation [19]. To save computational time, particle/-particle interactions are neglected in the given case. The particles are released 5 mm below the edge of the melt delivery tube over a radius of 2 mm corresponding to the area of particle creation in the atomization experiments.

For the calculations without coaxial gas, a 2D model was used with the same conditions as in the 3D case to. The model itself is a stationary calculation of the flow using a linear solver [20] calculating the velocity and pressure separately to the turbulence.

4.2. Mesh size independency

To ensure that the calculated results show no grid size dependency, the centerline velocity and the velocity close to the wall were plotted against the nozzle distance for different number of computational cells for a gas only single-phase flow. The centerline velocity and the velocity close to the wall (distance to the wall is 5 cm) were chosen to ensure that the grid resolution of the high-speed region close to the nozzle, as well as the far slower velocities within the recirculation zone are satisfactory well calculated. The results are given in Fig. 6.

Both plots show a convergent behavior with $6{\cdot}10^5$ cells and more. The magnitude of the velocities as well as the position of the extreme values of the velocities in terms of nozzle distance are converging. These trends show that with a cell count $6{\cdot}10^5$ the grid is sufficiently fine to acquire calculation results without being influenced by the grid size.

5. Results

The first part of the results sections discusses the gas velocity measurements and the comparison of the measured velocities with the calculated velocity for the CFD model validation. The second part of the results presents the calculated velocity fields and the particle trajectories for different particle sizes with and without the usage of the coaxial gas. At the end the produced powder quality is discussed based on the particle size distribution and the particle circularity.

5.1. Model results

A comparison between the measured and the calculated gas velocities in a straight cylindrical chamber with a diameter of 0.7 m and a height of 4.8 m is used as validation for the model to further ensure the model capability of representing the flow pattern correctly. Following the gas flow, the particle trajectories are discussed for three different particle sizes each to estimate the change in trajectories.

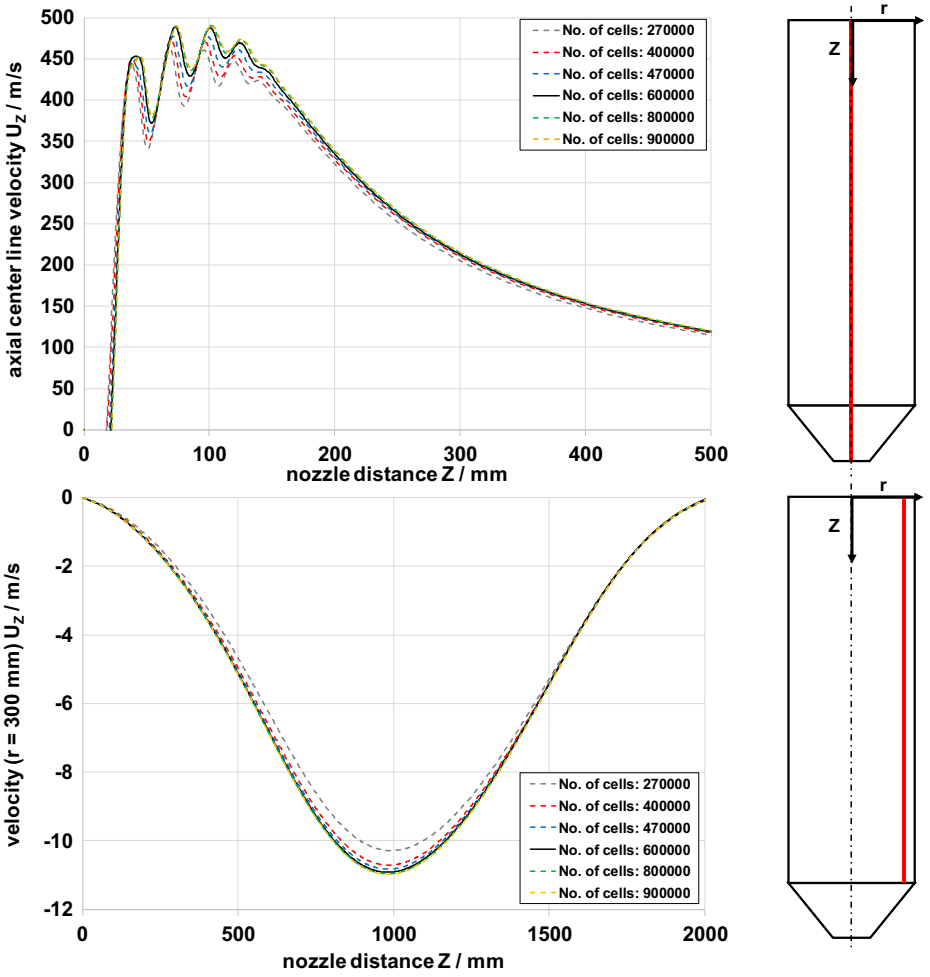

Fig. 6. Investigation of grid size impact on the calculated gas velocities on the center line (top; downward flow) and in the recirculation zone (bottom; upward flow).

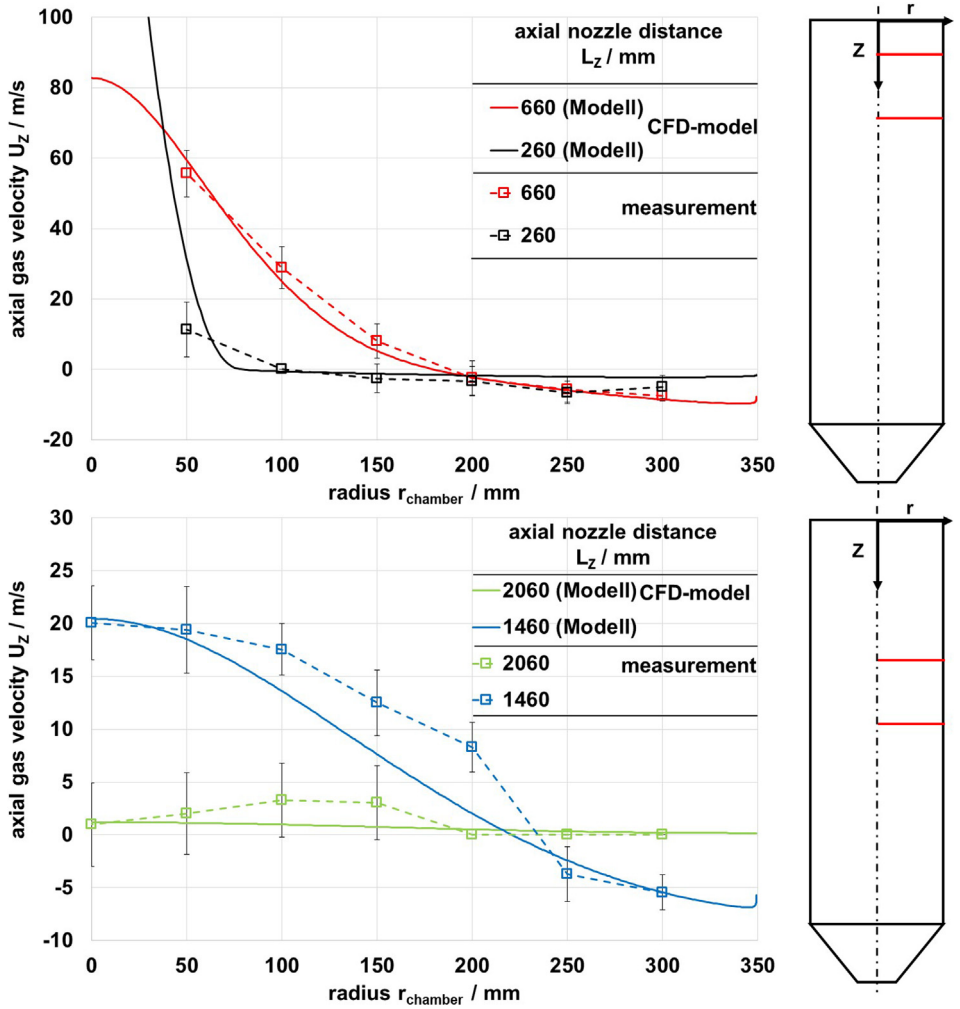

Fig. 7. Comparison of the measured gas velocities (symbols with dashed line) within the spray chamber and the calculated velocity (dotted lines) from the model for different nozzle distances. The gas mass flow was around 450 kg/h.

5.1.1. Validation

Fig. 7 shows the axial gas velocity versus the chamber radius for different nozzle distances. The solid lines represent the calculated velocities, the square shaped markers the measured velocities.

The results show the typical jet velocity structure with the highest velocities on the center line and a decrease in velocity with an increase in nozzle distance. This behavior is visible for the calculations as well as for the measurements. With an increase in nozzle distance, the jet broadens and develops a Gaussian like bell shape velocity profile. At a certain radius, the velocity changes direction from downstream to an upstream flow. This happens at a radius of 75 mm closest to the nozzle (axial nozzle distance of 260 mm) and at 250 mm radius for the 2060 mm nozzle distance. The change in velocity direction indicates the formation of a toroidal shaped recirculation zone (see 5.1.2). The measurement tends to underestimate the higher velocities and shows a larger error for velocities above 50 m/s. In general, comparison of the measurements with the calculations show a good agreement. This is especially true for the important recirculation area close to the wall.

5.1.2. 2D axially symmetric flow structure without co-flow

The flow structure of the gas flow field without coaxial gas is calculated in the axially symmetric case. The streamlines (color indicating the gas velocity) are shown in Fig. 8 in different area magnification levels.

The general flow structure and the gas velocity (colors) plotted as the z-component of the resulting velocity (a). The color range is limited between 10 m/s downstream and −10 m/s upstream velocity to get a better insight of the different flow areas. In (b) the top region with the recirculation zone is shown, as a streamline plot. The streamline plots (a) and (b) show that the recirculation mentioned before in 5.1.1 is forming in the upper half of the spray chamber and spreads down to approx. 2000 mm in downstream direction. This recirculation is developed due to the enclosing of the jet. Here, the entrainment of the gas jet cannot be satisfied by feeding gas from outside the system. Thus, the entrainment leads to lower pressures at the side of the jet. This is compensated by gas streaming from the bottom part of the jet back to the top. In (b) it is visible, that the center of recirculation zone is around 200 mm in radial direction. The recirculation zone shows an inclination inward. This may be explained by the velocities, where the directional change shifts from 75 mm to 250 mm with an increase in nozzle distance and is generally following the broadening of the jet due to the entrainment.

5.1.3. Particle behavior

To estimate the impact of the gas flow on the particle behavior, the particle trajectories were calculated for different particle sizes. The particle release area is 5 mm below the melt orifice surface. The chosen particle sizes are 1 μm, 10 μm and 54 μm (averaged mass median diameter derived from the experiments, see

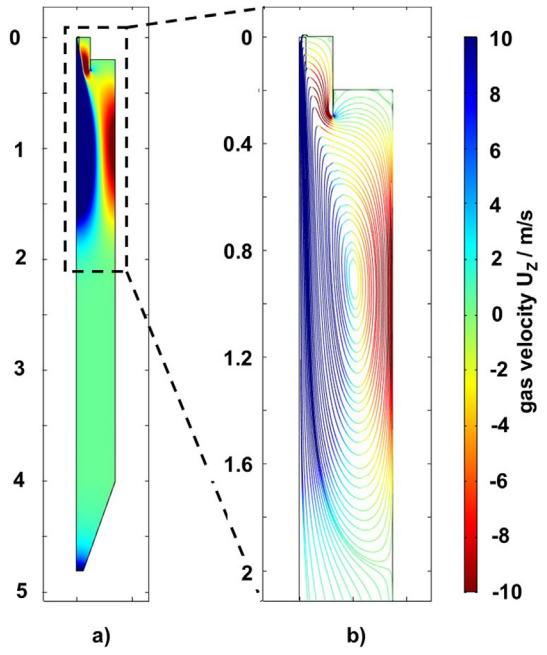

Fig. 8. Streamlines and axial velocity component u_Z (a) within the spray chamber for a gas mass flow of 450 kg/h. The created recirculation zone is shown in (b).

Table 5-1). The diameters represent the small, medium and large particle sizes found in the generated powders.

The results without the coaxial gas are shown in Fig. 9. The trajectories of (a), (b) and (c) are, showing the differences between the three particle sizes. For (a) and (b) the particles are accelerated in the nozzle region by the gas jet. A portion of the particles follows the gas flow towards the outlet while another portion of the particles is transported in the recirculation eddy and is mixed back into the atomization zone. In contrast to the small and medium particles, the 54 μm particles shown in (c) undergo acceleration and are forwarded directly to the outlet. The velocities shown by coloring of the trajectories indicate that the 54 μm particles are keeping their velocity over a larger distance due to their mass and hence higher inertia compared to the small and medium particles. They are therefore mostly unable to follow the redirection of the gas flow in the recirculation zone. Looking more closely at the top part of the spray chamber for the 1 and 10 μm particles shows differences in their behavior. Both particle sizes can reenter the atomization zone. While the 1 μm particles can almost reach back into the atomization area directly beneath the melt orifice, the 10 μm particles are only recirculating to a nozzle distance of 200 mm. Comparing the trajectories and the streamlines from Fig. 8 shows that this behavior is due to the fact that the 1 μm particles are still able to follow the gas flow while the 10 μm particles are drifting further into the center of the gas flow due to inertia and are getting accelerated downstream again.

5.1.4. 3D flow structure with co-flow

The influence of a tangential gas flow on the flow pattern within the spray chamber is analyzed in the 3D simulations. The resulting flow field by means of a 2D-plot of the flow field is given in Fig. 10 (a). The figure shows the velocity component in z direction, where the downstream direction is positive.

The flow field shows the atomization gas jet at the top of the chamber (in blue). The gas jet is deflected to the left side of the chamber. An upwards face flow is located on both sides of the jet due to the entrainment. A downstream flow is located at the wall of the top part of the chamber. This flow is created by the tangential inlets. Additionally, downward facing flow areas are visible throughout the spray chamber along the chamber walls. In the center of the plane, an upward flow is visible until a nozzle distance of around 2.5 m. From there on the flow is in downstream direction across the full diameter of the chamber. The flow pattern is also indicated by the arrow plot in (b) with a focus on the upper area of the chamber. Here the afore mentioned entrainment close to the atomization jet is also clearly visible. This entrainment zone is likely to cause the upward facing flow in the center of the chamber. In Fig. 11 the corresponding 3D streamline plot of the atomization gas jet (a), (b) and the tangential gas flow is plotted. The color indication is for the z-component of the velocity.

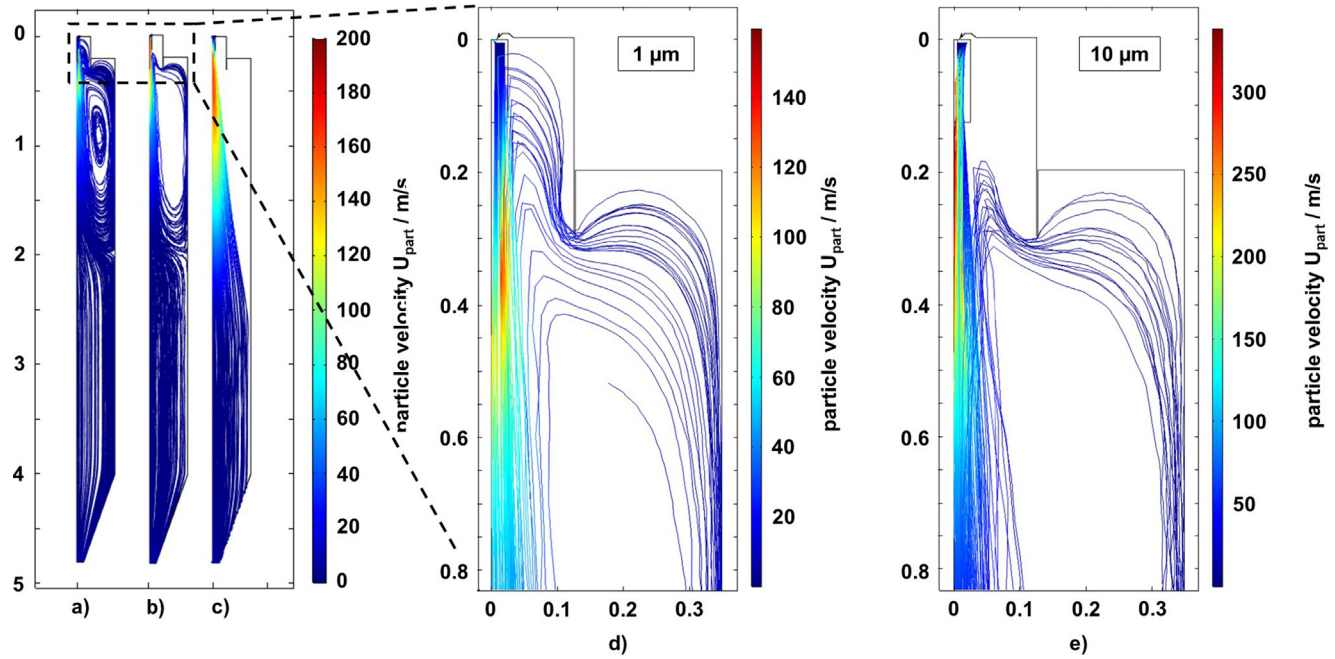

Fig. 9. Calculated particle trajectories for different particle sizes a) 1 μm b) 10 μm and c) 54 μm. The color scheme indicates the velocity magnitude of the given particles.

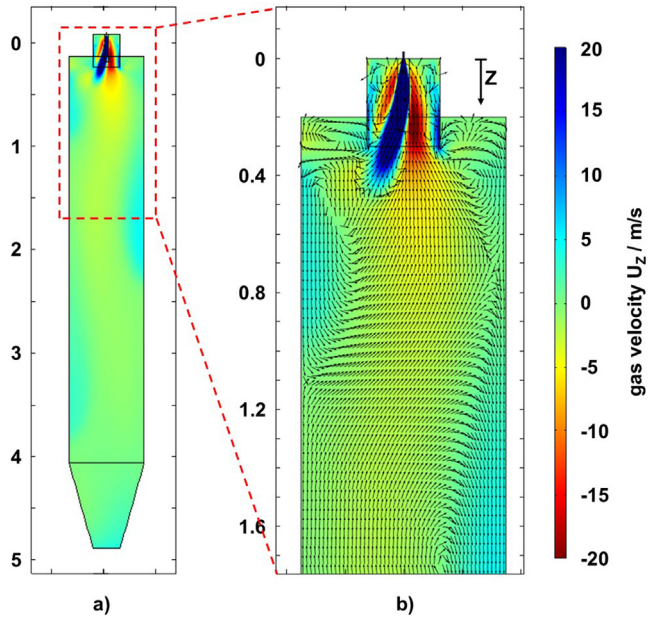

Fig. 10. Resulting flow pattern with coaxial gas, visualized on a 2D cut plane in the center of the spray chamber (a). The magnification (b) shows macro scale vortices along the chamber wall, induced by the movement and position of the atomization gas jet. The color scheme indicates the velocity in z-direction of the gas flow ranging from 20 m/s (downwards) up to −20 m/s (upwards). The arrows only indicate the direction of the gas flow.

The streamline plot (a) shows that the gas flow from the atomizer nozzle is spiraling downwards along the spray chamber walls. This flow corresponds well with the downwards facing areas in Fig. 8. The top view (b) in combination with the streamline plot in (c) emphasizes on the fact that this is caused by the swirl induced by the tangential gas flow (the streamlines are only give for one of the coaxial gas inlets to improve the visibility of the flow pattern therefore the second inlet is not visible in the given image).

5.2. Powder results

The experimental results are presented and discussed, as the achieved particle size distribution measured via static particle imaging, the measured particle circularity and scanning electron microscope (SEM) images.

The parameters of the experiments are shown in Table 5-1.

The experiments were conducted with an atomization pressure of 1.2 MPa leading to a gas mass flow of 450 kg/h ($\dot{M}_{atom}$). The melt orifice diameter was 2.5 mm. The atomization was done with nitrogen and an AISI52100 steel. The pouring temperature was 1941 K and the residence time at that temperature was 10 min. The varied parameter was the use of coaxial gas. For a statistical quality, three experiments were done with and without coaxial gas.

The resulting particle size distributions are shown in Fig. 13. The diagram shows the accumulated number size distribution plotted against the particle diameter.

5.2.1. Scanning electron microscope (SEM)

The SEM images shown in Fig. 12 give an impression of the shape and the surface property of the sprayed particles. When using SEM images, one should consider that they can only give a small and not representative sample on the particles. Therefore, SEM images should be used in combination of additional data given for example by the results in Fig. 13 and Fig. 14.

Three different particle size fractions are shown to emphasize the difference between the size classes. On the left-hand side, particles sprayed without coaxial gas are shown and on the right-hand side are the corresponding coaxial gas sprayed particles. All are inherently spherical and smooth when it comes to shape and surface. It is also visible, that all six samples show satellite particles on the primary particle surface, indicating that the change in circularity cannot only be influenced by the satellite particles. Comparing the different processes by looking at the size class from 0 to 20 µm shows no difference between the produced particles. On both sides satellite particles as well as deformed primary particles can be found. This impression is backed by the circularity measurement

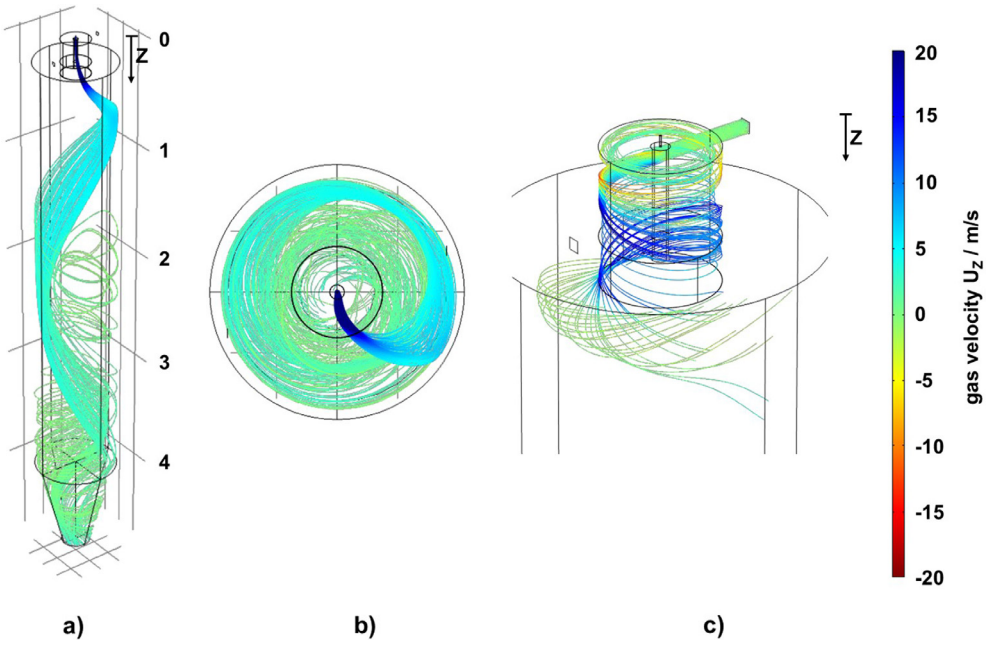

Fig. 11. Streamline plot of the atomization gas flow from an isometric perspective (a) and a top view (b), showing the displacement of the jet. The behavior of the atomizer jet is caused by the tangential gas flow (c) inducing a swirl flow within the spray chamber.

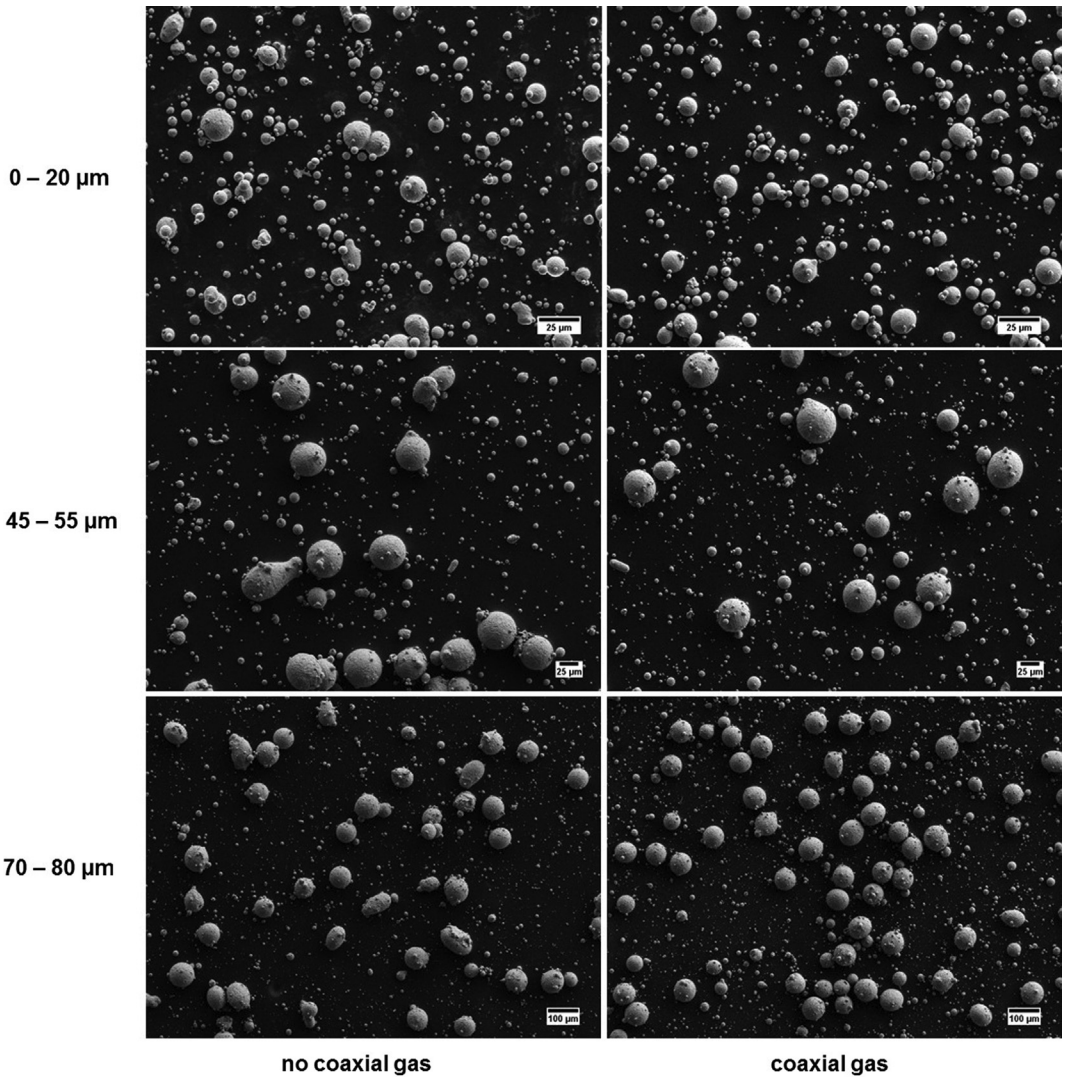

Fig. 12. SEM images taken for three different size fractions of the produced powders with and without coaxial gas influence.

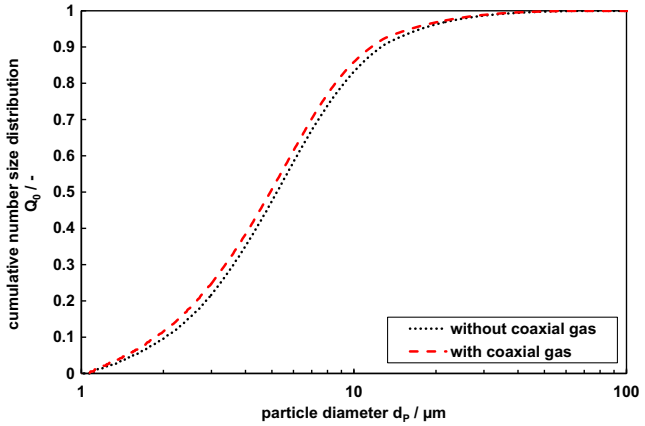

Fig. 13. Cumulative number size distribution of metal powder with and without coaxial gas.

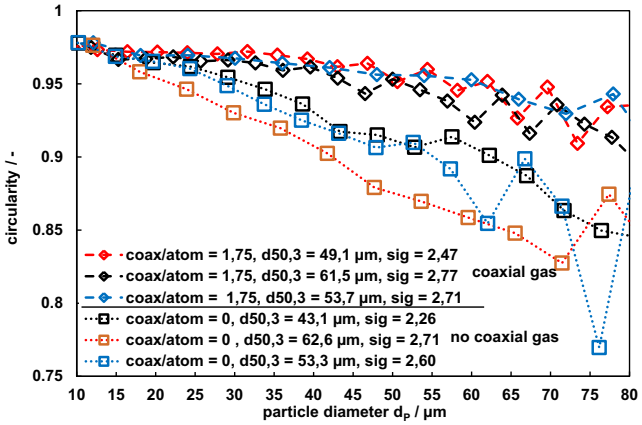

Fig. 14. Comparison of the measured particle circularity with and without coaxial gas influence for a AISI54100 steel.

where differences in the measured circularity are starting with particles above 20 µm. Nonetheless, the measurement also shows that circularity in this size class is already high compared to the other size classes. Due to shorter cooling and solidification times of smaller particles the influence on the circularity is mainly driven by the amount of satellites and the building of aggregates.

Comparing the powders in the size class from 45 to 55 µm show differences in the shape depending on the process. The larger par-

ticles produced with coaxial gas show less deformation of the primary particles compared with the particles produced without the coaxial gas. A difference in satellite occurrence cannot be derived by the SEM images. The same impression is given by the depiction of the particle size class from 70 to 80 μm. Again, the particles produced with coaxial gas show less deformation but still a certain amount of satellite particles are clearly visible for both powders in this size range. The improvement of shape visible in the SEM images for the larger particles behavior is in line with the measurement results given in Fig. 13. Here the circularity shows strong differences between the powders in the larger particle size classes depending on the process.

5.2.2. Particle size

The particle size has been measured for each experiment and the three particle size distributions from the experiments with and without coaxial gas have been averaged, resulting in the two curves shown in Fig. 13. The given diameter is the circle equivalent diameter, which is the diameter of a perfect circle with the same projection area of the measured particle.

Both powders show a particle number median diameter close to 5 μm. It can be seen, that the use of coaxial gas is leading to a shift to smaller particle sizes in general. This indicates a larger number of smaller particles within the powder. A reason for this behavior might be a decrease of satellite particles on the primary particles. Instead the former satellite particles are now separated particles within the powder.

5.2.3. Particle morphology

The particle shape measurements by means of the particle circularity are given in Fig. 14. Here, the averaged circularity is plotted against the particle diameter. The circularity Ci is defined as:

$$Ci = \frac{4\pi r}{P^2} \tag{1}$$

With r as the radius of circle and P as the perimeter. The curves show the identical trends as the circularity decreases with an increase in particle size. For a particle size of 5 μm the circularity is at about 0.97 for all powders independently of coaxial gas usage. The powders produced using coaxial gas are then decreasing to a circularity between 0.9 and 0.95 for a particle diameter of 80 μm. The particles created without the coaxial gas are showing the same trend but with a steeper gradient. The circularity for 80 μm particle diameter is between 0.87 and 0.85. A significant difference in circularity for a given particle diameter starts at 15 μm. Below that no difference is visible in the circularity behavior of the powders.

6. Conclusions

In this work the impact of the gas flow pattern, within powder production of metal particles for additive manufacturing by spraying, on the particle shape and particle circularity has been examined by modeling and simulation of the two-phase flow in the spray chamber. The impact of changing the flow structure due to the use of an auxiliary coaxial gas flow in the spray chamber is analyzed. The macro scale flow pattern within the atomization chamber was modeled. The gas flow was validated with velocity measurement data from the experimental setup. The resulting particle trajectories have been calculated for different particle sizes. A proper model was set up for the coaxial gas simulation to investigate the change of the flow pattern for a fixed atomization to coaxial gas flow ratio.

Corresponding atomization experiments have been conducted with and without coaxial gas flow. The resulting particles size and circularity distributions were measured with laser diffraction and particle imaging. The particle shape was also examined with SEM imaging for three different size classes.

The results of the particle measurements show a shift to smaller particle sizes when using coaxial gas, indicating a larger number of smaller particles within the powder. The coaxial gas results in a certain number of small particles that usually adhere to primary particles and building satellites, thus decreasing the general particles size. The circularity of the powders shows that for particles above 15 μm in diameter the use of coaxial gas leads to a reproducible increase in particle circularity. The increase is up to ten percent for large particles. This result is confirmed by the SEM analysis, where in the medium and large size fraction less deformed particles occur. A change in the number of satellite particles has been found within the atomization process for metal powder production with changing process conditions. Basic observations have been done in pictures of particle fractions where an increased number of single smaller particles in the background of the medium and large size fractions are found. In addition, slight changes in the particle size distribution have been observed that are attributed to the change in satellite particle formation with changing process conditions. The change in the particle size distribution and particle shape when using additional coaxial gas may be explained by the general diluting effect of the chamber atmosphere. In this case i.e. that the additional coaxial gas flow changes the trajectories of particles (depending on their diameter) and reduce the particle concentration resp. the number of particles within certain spray chamber areas (e.g. close to the nozzle). This effect decreases the collision probability of the particles, which may lead to a smaller number of deformed particles due to particle/particle collisions, as well as to a smaller number of aggregated satellite particles on primary particles. Since smaller particles still are produced in the atomization process itself, this diminished aggregation rate can also be seen by the increased number of individually detected smaller particles in the particle size distribution. A significant influence of the change in gas temperatures due to the coaxial gas on the particle circularity can be neglected. Ciftci et al. 2016 [21] showed that even when using hot gas for atomization, there is no significant influence on the resulting particle shape for certain alloys. Therefore, the changes in the psd found are attributed to the change in gas flow pattern in the spray tower and the related change in the particle trajectories. Additionally, the analysis of the number distributions seems to be a good approach to evaluate the occurrence of aggregated satellite particles and can be used to distinguish between a general change in particle shape and a change in satellite aggregation on the particles. This cannot be done with shape factors alone due to the limitation of optical resolution in light microscopy or the low number of particles one can analyze via SEM leading to a sample size that is not fully representing the powder produced.

Acknowledgement

This investigation is funded by Deutsche Forschungsgemeinschaft (DFG, German Research Foundation) – project number 276397488 – SFB 1232 (Farbige Zustände). The funding is gratefully acknowledged.

References

[1] K. Danjo et al., Effect of particle shape on the compaction and flow properties of powders, Chem. Pharm. Bull. 37 (11) (1989) 3070–3073.
[2] O. Ozcan, M. Ruhland, W. Stahl, The effect of pressure, particle size and particle shape on the shear strength of very fine mineral filter cakes, Int. J. Miner. Process. 59 (2) (2000) 185–193, https://doi.org/10.1016/S0301-7516(99)00064-2.
[3] X. Fu et al., Effect of particle shape and size on flow properties of lactose powders, Particuology 10 (2) (2012) 203–208.

[4] D. Hann, J. Stražišar, Influence of particle size distribution, moisture content, and particle shape on the flow properties of bulk solids, Instrum Sci. Technol. 35 (5) (2007) 571–584.
[5] V. Uhlenwinkel, H. Henein, U. Fritsching, Metal Sprays and Spray Deposition, Springer, 2017.
[6] H. Lubanska, Correlation of spray ring data for gas atomization of liquid metals, J. Met. 22 (1970) 45.
[7] U. Fritsching, Droplets and particles in sprays: tailoring particle properties within spray processes, China Particuol. 36 (12) (2005) 125–133.
[8] J. Bruce See, G.H. Johnston, Interactions between nitrogen jets and liquid lead and tin streams, Powder Technol. 21 (1) (1978) 119–133.
[9] O.S. Nichiporenko, Y.I. Naida, Heat exchange between metal particles and gas in the atomization process, Soviet Powder Metall. Metal Ceram. 7 (7) (1968) 509–512.
[10] L. Achelis, V. Uhlenwinkel, Characterisation of metal powders generated by a pressure-gas-atomiser, Mater. Sci. Eng., A 477 (1–2) (2008) 15–20.
[11] L. Huang, K. Kumar, A.S. Mujumdar, Use of computational fluid dynamics to evaluate alternative spray dryer chamber configurations, Drying Technol. 21 (3) (2003) 385–412.
[12] L. Huang, K. Kumar, A.S. Mujumdar, A parametric study of the gas flow patterns and drying performance of Co-current spray dryer: results of a computational fluid dynamics study, Drying Technol. 21 (6) (2003) 957–978.
[13] A. Lampa, U. Fritsching, Spray structure analysis in atomization processes in enclosures for powder production, Atomization Sprays 21 (9) (2011) 737–752.
[14] M. Mezhericher, A. Levy, I. Borde, Probabilistic hard-sphere model of binary particle–particle interactions in multiphase flow of spray dryers, Int. J. Multiph. Flow 43 (2012) 22–38.
[15] D. Schwenck et al., Generation of small batch high quality metal powder, Powder Metall. 57 (3) (2014) 171–175.
[16] D. Schwenck et al., A novel convergent–divergent annular nozzle design for close-coupled atomisation, Powder Metall. (2017) 1–10.
[17] Y. Saad, M.H. Schultz, GMRES: A generalized minimal residual algorithm for solving nonsymmetric linear systems, SIAM J. Sci. Stat. Comput. 7 (3) (1986) 856–869.
[18] S.K. Rathore, M.K. Das, Comparison of two low-Reynolds number turbulence models for fluid flow study of wall bounded jets, Int. J. Heat Mass Transf. 61 (2013) 365–380.
[19] C.T. Crowe et al., Multiphase Flows with Droplets and Particles, CRC Press, 2011.
[20] O. Schenk et al., PARDISO: a high-performance serial and parallel sparse linear solver in semiconductor device simulation, Future Generat. Comput. Syst. 18 (1) (2001) 69–78.
[21] N. Ciftci et al., Impact of hot gas atomization on glass-forming alloys, World PM 2016, European Powder Metallurgy Association, Hamburg, 2016.